Journal of Physics and Chemistry of Solids 170 (2022) 110955

Contents lists available at ScienceDirect

Journal of Physics and Chemistry of Solids

journal homepage: www.elsevier.com/locate/jpcs

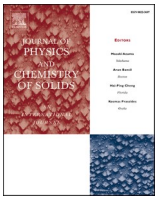

FLA

In-situ electron loss spectroscopy reveals surface dehydrogenation of hydrated ceria nanoparticles at elevated temperatures

Annett Thøgersen [a,*], Xinwei Sun [b], Ingvild Thue Jensen [a], Øystein Prytz [c], Truls Norby [b]

[a] SINTEF, Materials Physics, Forskningsveien 1, Oslo, NO-0373, Norway
[b] University of Oslo, Department of Chemistry, Centre for Materials Science and Nanotechnology, FERMIO, Gaustadalléen 21, Oslo, NO-0349, Norway
[c] University of Oslo, Department of Physics, Centre for Materials Science and Nanotechnology, Box 1048 Blindern, Oslo, NO-0316, Norway

ARTICLE INFO

Keywords:
ETEM
EELS
Ceria
Microscopy
Nanopowder
Hydrogen

ABSTRACT

Ceria (CeO_2) exhibits high reversible oxygen storage capacity at intermediate temperatures (500–800 °C) related to an extraordinary and not fully understood reduction of its surfaces. We have investigated pristine and alcohol-dispersed commercially available ceria nanoparticles by in-situ scanning transmission electron microscopy with electron energy loss spectroscopy (STEM-EELS) to examine the dynamic changes during the initial redox reaction process of ceria nanoparticles in an ultra-high vacuum atmosphere using an in-situ heating holder. High spatially resolved EELS was used to estimate the amounts of Ce^{3+} and Ce^{4+} in the nanoparticles as a function of temperature, based on the white-line ratios M_5/M_4 of the EELS spectra. The results show a nm-range thick surface layer rich in Ce^{3+} on pristine particles prior to heating. During heating, this oxidises to Ce^{4+}. Heating in high vacuum should normally not lead to oxidation, but the observed results can be understood if the surface layer has an oxyhydroxide composition such as CeOOH, which by heating in the vacuum dehydrogenates and hence oxidises to CeO_2, a process that requires diffusion of hydrogen only. This process occurred for all samples, but was more pronounced for the particles that were previously dispersed in ethanol. Thermogravimetric analysis (TGA) by heating the pristine powder in dry atmosphere yielded a considerable weight loss confirming the content of hydroxide and probably water in and on the CeO_2 particles. The results suggest that CeO_2 surfaces are reduced to a layer of oxyhydroxide by hydrogen-containing molecules like water vapour or alcohols.

1. Introduction

Ceria (CeO_2) nanoparticles find use in applications such as oxygen sensors, solid oxide fuel cells, and three-way catalysts to remove NOx and CO from combustion exhausts [1–3], owing to the oxide ion conductivity, electronic structure, and variable stoichiometry.

Ceria particles exhibit high and reversible oxygen storage capacities by changing the valence state of Ce between +4 and +3 in the surface at intermediate temperatures (500–800 °C). The reduced state involves oxygen vacancies and electrons (representing Ce^{3+}) introducing oxide ion and electronic conductivity in the surface [4,5]. The separation of the Ce^{3+} and Ce^{4+} components can be carried out by peak fitting the electron energy loss spectra (EELS) $M_{4,5}$ peak using transmission electron microscopy (TEM), as well as measuring the white line intensity ratio [4,5]. For pure ceria, the reduction from +4 to +3 was found to occur by heating above 730 °C, in a hydrogen rich atmosphere [4]. Most studies on the temperature evolution of ceria particles have therefore been made at high temperatures. Previous TEM investigations of the surface of ceria have shown a thin layer of Ce^{3+} [4,6–8]. Studies have also shown that investigating the particles under high vacuum produces more Ce^{3+} on the surface than if investigating the particles in an oxygen atmosphere [9,10]. Baalousha et al. [11] and Wu et al. [11] found that ceria nanoparticles have more Ce^{3+} than larger particles and bulk ceria. It is important to map the compositional variations on the nanoparticle surface in-situ at low temperatures, as reduced ceria nanoparticles may be unstable and small changes may have a big influence in the catalytic functionality of the particles [4]. We have therefore investigated the composition of pristine ceria nanoparticles as well as the composition of ceria dispersed in alcohols prior to analysis, which is the most common way of preparing and dispersing nanoparticles for TEM analysis.

2. Methodology

Ceria nanoparticles from Sigma-Aldrich Co. were used for the ex-

* Corresponding author.
E-mail address: annett.thogersen@sintef.no (A. Thøgersen).

https://doi.org/10.1016/j.jpcs.2022.110955
Received 27 April 2022; Received in revised form 6 August 2022; Accepted 8 August 2022
Available online 27 August 2022

periments (Cerium (IV) Oxide nanopowder, Pcode: 1001924131, <25 nm particle size). For the in-situ heating measurements, a *Protochips* Fusion holder was used. TEM samples were prepared by dispersing dry ceria powder or a drop of ceria mixed with either isopropanol or ethanol on a Protochips in-situ heating chip. The samples were analysed by a probe corrected and monochromated FEI Titan G2 60–300 microscope operated at 300 kV, using high resolution scanning TEM (STEM), electron energy loss spectroscopy (EELS) with a Gatan imaging filter and detector, and Super-X energy dispersive spectroscopy (EDS). In order to reduce beam damage, electron beam current of less than 0.1 nA was used. In some of our experiments we also performed a double analysis of each particle in the heating test to see if there were any changes in our results after the spectral image EELS acquisition. No damage was observed in our extra tests. The EELS spectra were acquired using dual EELS spectrum image (SI), in order to avoid referencing issues. This means that we acquire a low loss EELS spectrum with the zero-loss peak together with the core-loss EELS spectrum of the Ce-$M_{4,5}$ peak, and using the zero-loss peak as the referencing peak. The post acquisition data processing was performed using Digital Micrograph from Gatan Inc. and CasaXPS for peak fitting analysis. More details on the peak fitting is given in the Results chapter.

In-situ heating was performed with temperature steps of 0.05 °C per second, for then to wait about 10 min (before taking EELS spectra) to avoid drift due to heating. EELS spectra were acquired with either a 0.25 eV/ch dispersion (collection semi-angle 12 mrad and convergence semi-angle 21 mrad), or with a 0.1 eV/ch dispersion (collection semi-angle 100 mrad and convergence semi-angle 30 mrad), with some variations in spectrum image pixel size.

Thermogravimetric analysis (TGA) was made with a Netzsch 449 F1 Jupiter® thermal analyser (Netzsch GmbH, Germany) on the as-received CeO_2 nanopowder, uniaxially pressed at 3 MPa into a pellet. The sample was first dried at 26 °C in N_2 gas for 3 h. It was further dried and degassed during stepwise heating to 400 °C at 3 K/min, and then held at 400 °C for 6 h to ensure complete removal of water and hydrogen and any organic residue from the surface. The weight increase was then measured by flowing wet (pH_2O = 0.026 atm) N_2 over the sample at 400, 125 and 26 °C during cooling. The relative increase in weight and corresponding uptake of water is calculated on the basis that the content of adsorbed water and other gases in dry N_2 at 400 °C was zero.

3. Results

The shape and sizes of the ceria nanoparticles studied in this work are shown in the STEM images in Fig. 1 A and E, with the corresponding electron diffraction images in B and D. The diffraction pattern in Fig. 1B is consistent with the CeO_2 crystal structure with a space group of Fm-3m (225) in the [110] zone axis. Diffraction of several particles in (E) shows ring patterns resulting from many crystal orientations, all corresponding well to the CeO_2 structure. A 1:2 compositional relationship between Ce and O was also confirmed by EDS.

The content of Ce^{3+} in the samples may be affected by the treatment of the ceria nanoparticles prior to the analysis. We have therefore investigated ceria treated in three different ways common to the TEM-sample preparation process namely, as-received (pristine) ceria powder and ceria dispersed in ethanol or isopropanol. EELS spectra in Fig. 2 shows spectra taken from bulk and surface of our caria nanopowder, with a clear Ce^{3+} and Ce^{4+} signature. Even though there may be minor Ce^{4+} and Ce^{3+} present in the spectra as well, these spectra shows the signature shapes we are analyzing in this paper. The spectra are composed of the two peaks, due to spin-orbit splitting, (white lines) $M_{4,5}$. These lines are caused by excitations from the $M_{4,5}$ (3d) to the unoccupied states in the N(4f) band, reflecting changes in the occupancy of the 4f band and thereby also the oxidation state [4]. The EELS Ce-$M_{4,5}$ peaks have been peak-fitted with Gaussian-Lorentzian peaks corresponding to Ce-M_5 and Ce-M_4, where the Ce-M_5 and Ce-M_4 peaks of Ce^{3+} are located at energy losses of 880.1 eV and 898 eV respectively, with an energy separation of about 17.9 ± 0.2 eV. For the Ce^{4+} component, the Ce-M_5 peak is located at 881.4 eV and Ce-M_4 peak at 899.6 eV, with an energy separation of about 18.2 ± 0.2 eV. Intensity ratios of the M_5 to M_4 white lines of Ce^{3+} was found to be 1.3 (I_{M_5}/I_{M_4} = 1.3.), while for Ce^{4+} the intensity difference is I_{M_5}/I_{M_4} = 0.8. A variation in-between these two numbers can be related to a change in oxidation state.

We have used the zero-loss peak (from dual EELS) for initial energy referencing. However, due to some misalignment of the drift tube or the image filter, we also experienced a shift in the peaks between samples dispersed in ethanol and isopropanol. In order to more easily compare the peaks we aligned the 3+ peaks for the samples at room temperature. The analysis has been carried out for eight different particles, and the results of some of them are presented in the following sections.

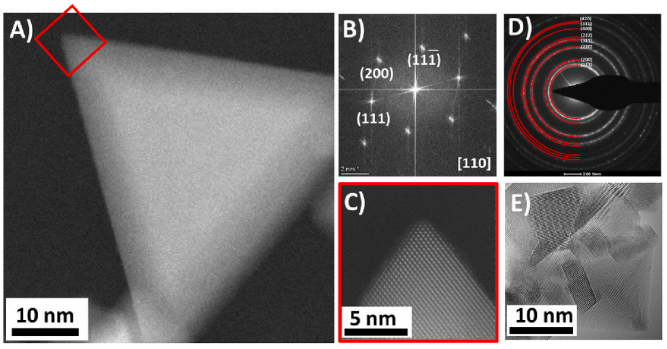

Fig. 1. A) HAADF STEM image of a CeO_2 nanoparticle, B) corresponding electron diffraction pattern, C) high resolution HAADF STEM image, D) electron diffraction pattern from E), and E) STEM image of many CeO_2 particles.

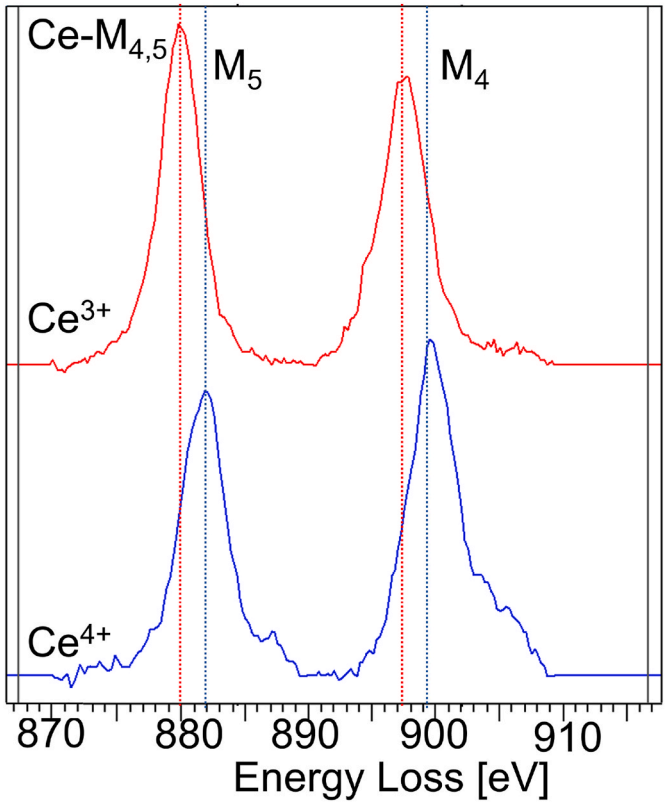

Fig. 2. EELS spectra of the Ce-$M_{4,5}$ peak, in an area with mainly Ce^{3+} and Ce^{4+} showing the different spectral signatures.

3.1. Pristine CeO_2-powder

We examined four pristine particles at 25 °C, 200 °C, and 400 °C, where most of the changes in composition were found to occur. Only the spectra and images of one of the particles will be presented, while the data of the other three nanoparticles are plotted in Section 3.4.

EELS spectra of the pristine ceria particle is shown in Fig. 3A and B, from the whole particle and from the surface layer respectively. The percentages of Ce^{3+} at the corresponding temperature, as well as the estimated oxidation state based on the white line ratio are presented in Table 1. The pristine particle contains 53% Ce^{3+} in the whole particle at room temperature (estimated oxidation state of +3.3), and 80% Ce^{3+} at the surface, as shown in Fig. 3B. During heating in high vacuum, the Ce-$M_{4,5}$ peak moves to higher energy loss, and the white line intensity ratio shifts to a clear Ce^{4+} signature. At 400 °C, the particle contains only 13% Ce^{3+}, and we can observe 31% Ce^{3+} at the surface layer. Energy loss mapping of the integrated EELS signal of the Ce^{4+} and Ce^{3+} peaks presented in Fig. 4 shows that at room temperature the particle contains a mix of both Ce^{3+} and Ce^{4+}. During heating, most of the Ce^{3+} in the bulk particle transform into Ce^{4+}, while the transformation at the surface is not as quick, resulting in a layer of Ce^{3+} at the surface. This evolution profile was also found for the three other samples we have examined.

3.2. CeO_2-powder in ethanol solution

EELS spectra of ceria particles dispersed in ethanol prior to analysis are shown in Fig. 3C and D. At room temperature, the particle contains 71% Ce^{3+} (estimated oxidation state +3.3). The white line intensity ratio also shows a clear Ce^{3+} signature. During heating in high vacuum, we observe a clear shift in the Ce-$M_{4,5}$ peak to higher energy loss, as well as a shift in the white line intensity ratio to a pronounced Ce^{4+} signature. At 700 °C, the particle contains only 16% of Ce^{3+}. This can also be observed in the spectra from the surface (in Fig. 3D) where Ce^{4+} dominates at higher temperatures. Fig. 5 shows energy filtered images of the particle at the different temperatures. The result reveals that the Ce^{3+} is mainly found at the surface of the particle. There is also a clear decrease in Ce^{3+} at 400 °C.

3.3. CeO_2-powder in isopropanol solution

EELS spectra of ceria dispersed in isopropanol prior to analysis are shown in Fig. 3E and F. Ce^{3+} is observed at both the whole nanoparticle and the surface at room temperature, with 64% and 100% Ce^{3+}, respectively. Increasing the temperature shows a significant reduction in Ce^{3+} content of the whole particle, resulting in more Ce^{4+}. However, no significant decrease in Ce^{3+} is observed at the surface. The corresponding energy filtered image are shown in Fig. 6. The images show that at room temperature, Ce^{3+} is pronounced at the surface. During heating, Ce^{3+} is reduced overall in the particle.

3.4. Temperature evolution of the ceria samples

The composition of Ce^{3+} in the four samples as a function of temperature is shown in Fig. 7, for the whole particle (A) and for the surface (B). The error bars are estimated uncertainty/errors in the calculated oxidation state (y-axis, ± 0.1), and calculated composition from EELS data (y-axis, ± 4%), found by varying the fitting parameters and measurements of the spectra. All samples start with a relatively high amount of Ce^{3+} in the whole particle, which decreases with increasing temperature (Fig. 7A). The sample dispersed in isopropanol shows a small initial increase in the amount of Ce^{3+}, with a slight increase at 200 °C, before it decreases further.

The calculated oxidation state based on the white line ratio as a function of Ce^{3+} content is shown in Fig. 8, using data from all samples investigated. A linear thread-line is fitted to the data points and shows a near-linear evolution of the oxidation state, with a R^2 value of about 0.86 (a measurement of how good the line fits the data points, where 1 is the best). However, some of the data points are not connected to the

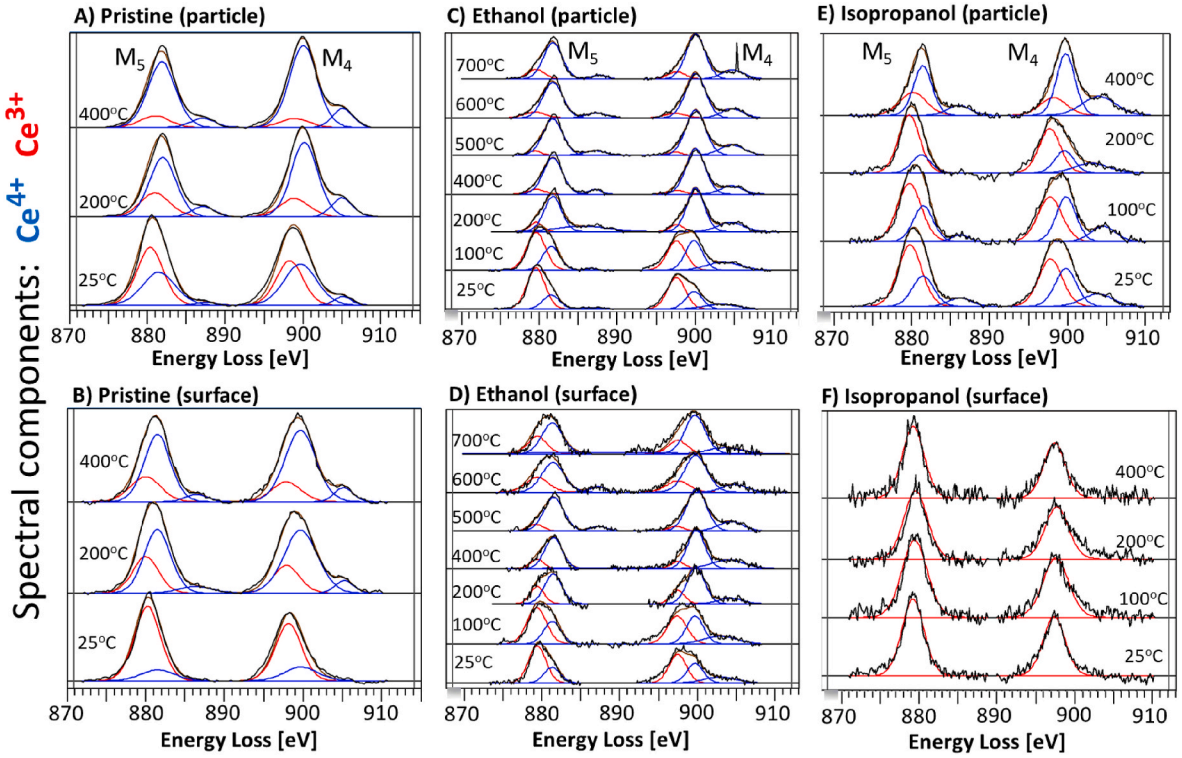

Fig. 3. EELS spectra of the Ce-$M_{4,5}$ peaks, both from the whole particle (A,C,E) and the surface (B,D,F), of pristine ceria particle (A and B), ceria first dispersed in ethanol (C and D), and ceria first dispersed in isopropanol (E and F), at 25 °C–700 °C. The component Ce^{4+} is shown in blue, $Ce^{3+}$is shown in red, and the black is the experimental spectra.

Table 1
Amount of Ce^{3+} present in pristine ceria, ceria dispersed in ethanol, and ceria dispersed in isopropanol, with the mean oxidation state (ox. state) calculated based on the white line ratio.

	Particle						Surface					
	Pristine		Ethanol		Isopropanol		Pristine		Ethanol		Isopropanol	
Temp.	Ce^{3+}	ox.	Ce^{3+}	ox.	Ce^{3+}	ox.	Ce^{3+}	ox.	Ce^{3+}	ox.	Ce^{3+}	ox.
(°C)	(%)	state	(%)	state	(%)	state	(%)	state	(%)	state	(%)	state
25	53	+3.3	71	+3.3	64	+3.3	80	+3.0	54	+3.4	100	+3.0
100			58	+3.5	61	+3.4			59	+3.6	100	+3.0
200	26	+3.6	13	+3.8	74	+3.1	24	+3.4	26	+3.7	100	+3.1
400	13	+3.8	8	+3.7	35	+3.8	31	+3.6	16	+3.9	100	+3.0
500			6	+3.7					11	+3.7		
600			13	+3.8					29	+3.7		
700			16	+3.7					29	+3.6		

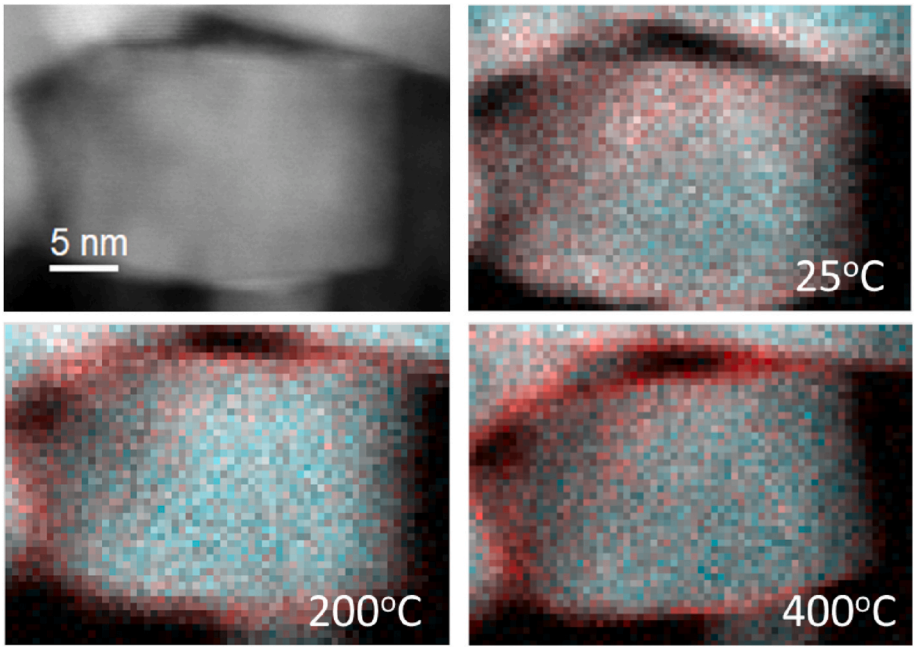

Fig. 4. STEM image of a pristine ceria particle, and EELS-mapping of the Ce^{3+} (red) and Ce^{4+} (blue) peaks at 25 °C, 200 °C, and 400 °C.

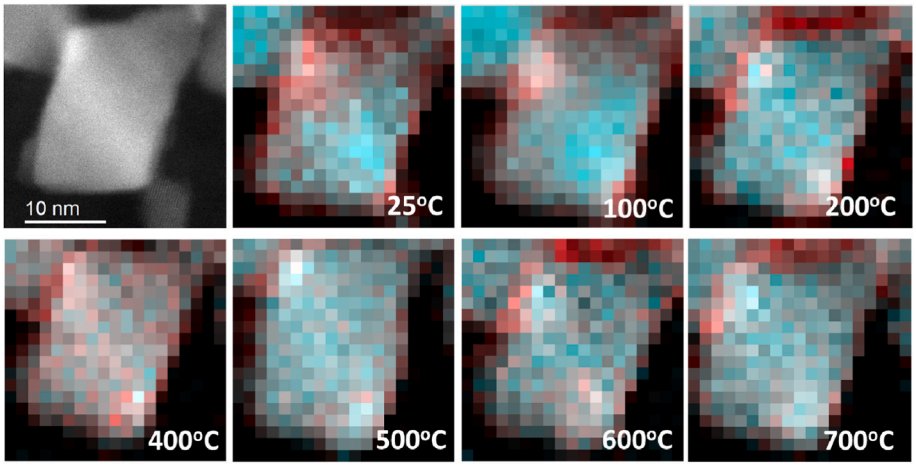

Fig. 5. STEM image of a ceria particle dispersed in ethanol, and EELS-mapping of the Ce^{3+} (red) and Ce^{4+} (blue) peaks at room temperature 25 °C, 100 °C, 200 °C, 400 °C, 500 °C, 600 °C, and 700 °C.

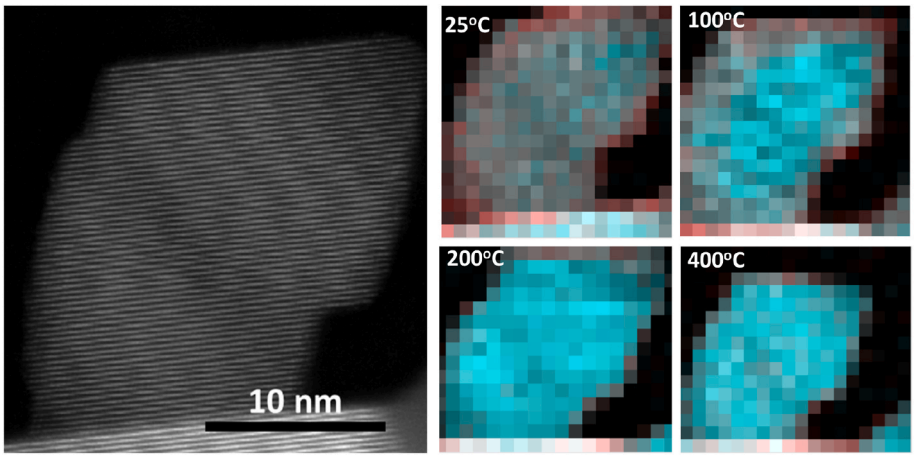

Fig. 6. A) STEM image of a ceria particle dispersed in isopropanol, and EELS-mapping of the Ce^{3+} (red) and Ce^{4+} (blue) peaks at room temperature (25°), 100 °C, 200 °C, and 400 °C.

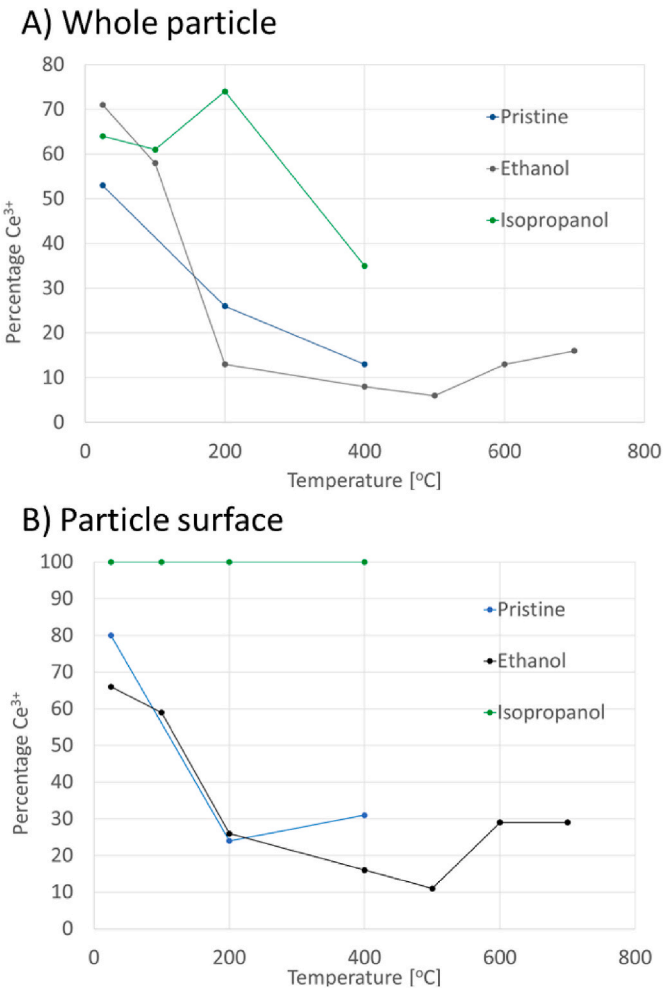

Fig. 7. Plot showing the fraction of Ce^{3+} present in A) the entire ceria particle, and B) ceria particle surface, with increasing temperature.

thread-line. From our experience, a combination of the oxidation state based on the white line ratio together with the fitted peaks is necessary to correctly determine the compositional profile of the samples.

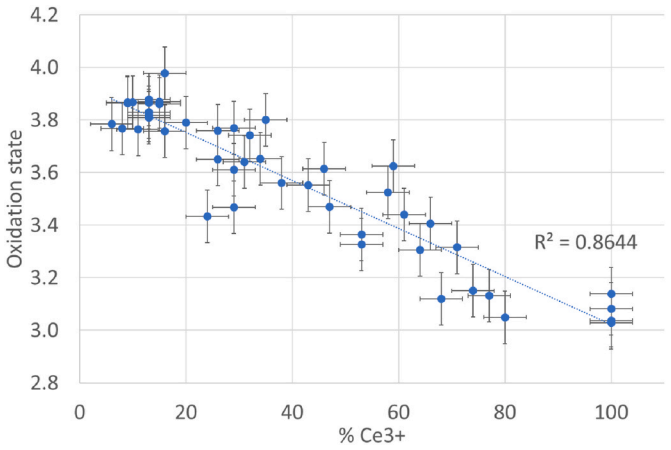

Fig. 8. A graph showing the average oxidation state found from using the white line ratio of the EELS Ce-$M_{4,5}$ spectra of the entire particle, as a function of the fraction of Ce^{3+} present in the sample found by peak fitting the EELS spectra of the different particles.

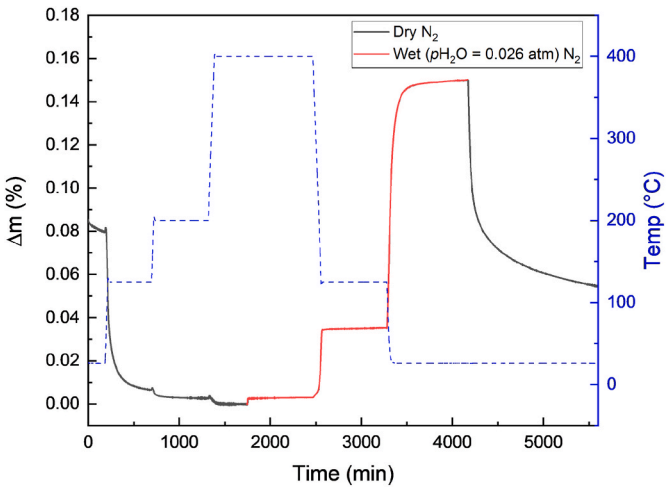

Fig. 9. Time-dependent mass change of CeO_2 under dry and wet (pH_2O = 0.026 atm) N_2 (left y-axis) in response to temperature change (right y-axis).

3.5. Thermogravimetry (TG)

The TG results for the temperature range 26–400 °C during heating in dry N_2 and cooling in wet N_2 are shown in Fig. 9. During heating under dry conditions, a significant amount of water is desorbed from the oxide upon heating to 125–200 °C, normally taken to reflect physisorbed water [12]. Further heating to 400 °C represents the removal of chemisorbed water, possibly also any water in the structure. In total, the water lost, supposedly present in and on the pristine CeO_2, amounts to around 0.092 mol H_2O per mol CeO_2. The amount of water adsorbed in the bulk of CeO_2 may be assumed to be negligible due to its unfavourable hydration thermodynamics. Therefore, the mass change may reflect adsorbed water. There may also be water or hydrogen left inside the crystallites from their synthesis. The following water uptakes in wet N_2 at 400, 125 and 26 °C correspond to approx. 0.003, 0.03 and 0.12 mol H_2O per mol CeO_2, respectively, in rough agreement with a previous report on CeO_2 powder with a specific surface area of 55 m^2/g [13].

4. Discussion

EELS results show that both pristine ceria as well as ceria dispersed in alcohols prior to analysis start with high amounts of Ce^{3+} at the surface of the particles. When heating in vacuum, this partly transforms into Ce^{4+}, where it is stable up to 700 °C. Johnston-Peck et al. [14] studied dose-rate-dependent damage of cerium dioxide by STEM-EELS. They found that when ceria is exposed to high beam damage, oxygen vacancies will form, and ceria will be reduced from +4 to +3 oxidation state. Since the particles in our study mainly experience a shift from +3 to +4 oxidation state, this process cannot be due to beam damage. The amount of Ce^{3+} and the evolution process during heating in the three types of samples are not significantly different, only a small increase in Ce^{3+} was found in the samples dispersed in ethanol. However, the amount of Ce^{3+} in the pristine samples is surprising. Heating in high vacuum should normally not lead to further oxidation. If the reoxidation to Ce^{4+} was due to annihilation of oxygen vacancies, it would require uptake of oxygen (which is not available in high vacuum) and lower temperatures (due to the negative entropy change of gas uptake). However, the results can be rationalized if the surface layer is an oxyhydroxide (based on the known stability of rare earth (III) oxyhydroxides) that we for simplicity represent as CeOOH, not oxide like Ce_2O_3 (both being Ce^{3+}). Dehydrogenation of a hydroxide yields hydrogen release, which is natural in the TEM vacuum, and it increases with temperature due to the positive entropy change of gas release. Thereby, when heating the particles in high vacuum, the surface layer dehydrogenates (oxidises) to CeO_2, a process that requires diffusion of protons only:

$$CeOOH \longrightarrow CeO_2 + \frac{1}{2}H_2(g)$$

The formation of the CeOOH layer is expected to happen under ambient conditions according to a reducing hydrogenation from water vapour:

$$CeO_2 + \frac{1}{2}H_2O(g) \longrightarrow CeOOH + \frac{1}{4}O_2(g)$$

Wang et al. [15] found the presence of hydroxyl groups (O–H) after water exposure of ceria surfaces. They suggest that these groups as well as hydrocarbons may also be absorbed from ambient environments. This will have a large effect on the wettability of the surface of ceria. The formation of a layer and not a complete hydrogenation of bulk CeO_2 suggests that the formation of a surface of CeOOH and the interface between CeO_2 and CeOOH, along with the associated charge separation and space charge layers, lowers the energy compared to a single CeO_2 surface. The growth of the layer then stops as soon as the surface attains bulk properties and/or the two space charge layers in the CeOOH layer meet.

This shows that H in CeO_2 is indeed present as H^+ compensated by Ce^{3+} in what may be termed CeOOH-like structures in a surface layer. If the TG results showing a loss of water from the pristine oxide of 0.092 mol H_2O/mol CeO_2 is interpreted as loss of H_2, this corresponds to as much as 0.83 mol H_2/mol CeO_2, or 1.66 H/CeO_2. It is hence likely that pristine CeO_2 nanoparticles have a mixture of H inside or on the surface, e.g. like regions or a layer of CeOOH, and H_2O adsorbed on the surface.

The existence of a layer of CeOOH on CeO_2 surfaces explains many observations, behaviours, and properties of CeO_2, e.g. redox and catalytic behaviour as well as protons found on the surface, but not bulk. The reasons why the surface phase has not been observed earlier may stem from the fact that it has the same oxygen content and a similar structure as the host CeO_2, and is very thin, requiring the use of TEM and the understanding gained by in-situ heating experiments.

We observed different evolution of the oxidation process for the different particles. Such differences have also been observed in the redox activity level [4,16]. Crozier et al. [4] reported that some particles were found to be inactive at room temperature and that heating till 700 °C in hydrogen resulted in no significant changes. Wang et al. [16] found that CeO_2–ZrO_2 solid solution nanoparticles with a large variation in concentrations through the particle were more active than homogeneous ones. They identified types of ceria nanoparticle behaviour depending on their redox activity level. In our case, with samples dispersed in alcohols, the evolution of the oxidation process may be dependent on the thickness of the CeOOH layer at the surface. The surface of ceria dispersed in isopropanol showed predominately Ce^{3+} with very little changes after heating. For particles dispersed in ethanol we observed both Ce^{3+} and Ce^{4+} at the surface, with a clear reduction upon heating. The ethanol sample has overall more Ce^{3+} in the whole particle at room temperature compare to the isopropanol sample, and it experiences a more abrupt decrease in Ce^{3+} content. The isopropanol sample on the other hand has still a large amount of Ce^{3+} left in the particle at 200 °C, located mostly at the surface. To our knowledge, such results have not been reported, and we recommend future studies on a larger set of particles to fully understand the difference between ceria dispersed in ethanol vs isopropanol.

5. Conclusion

We have found that during low temperature heating of ceria nanoparticles in vacuum, the oxidation state changes from +3 to +4 in a surface layer. There are small differences in the oxidation process between different particles, but at 400 °C and higher, they all have about the same compositional structure with mainly Ce^{4+}. This process occurs for both pristine sample and samples dispersed in alcohols. However, the Ce^{3+} content is much higher in the latter. Heating in vacuum should normally not lead to further oxidation, and our observations indicate that a layer of oxyhydroxide like CeOOH dehydrogenates to CeO_2, a process that only requires diffusion of H. This means that much of the Ce^{3+} we see on the surface is not a reduced oxide such as Ce_2O_3 but a reduced oxyhydroxide like CeOOH, i.e. the Ce^{3+} is not compensated by oxygen vacancies but by protons. These results are supported by TG results showing that the pristine CeO_2 powder contains a considerable amount of water and possibly hydrogen, probably partly adsorbed from ambient humidity and partly left from the synthesis of the powder. The use of in-situ TEM and EELS to map the evolution process of Ce^{3+} to Ce^{4+} in ceria nanoparticles has hence provided new insight to understand their properties, utilizing that the $M_{4,5}$ white line ratio gives good indication on the oxidation state of the particles.

Author statement

This is the individual author's contributions to the paper:

Annett Thøgersen: Data curation; Formal analysis; Funding acquisition; Investigation; Methodology (TEM/EELS work); Project administration; Main writer of manuscript/Review and editing.

Xinwei Sun: Data curation; Formal analysis; Investigation; Methodology (TG + samples), Writing part of manuscript and help with edit.

Ingvild Thue Jensen: Formal analysis; Investigation;

Øystein Prytz: Formal analysis; Funding acquisition; Project administration;

Truls Norby: Formal analysis; Funding acquisition; Supervision; Writing part of manuscript and help with edit.

Declaration of competing interest

The authors declare that they have no known competing financial interests or personal relationships that could have appeared to influence the work reported in this paper.

Data availability

Data will be made available on reasonable request.

Acknowledgement

Acknowledgement to Kathrin Michel, at Institute of Physical Chemistry, Justus Liebig University Giessen, for her contributions to this project. The Research Council of Norway (RCN) is acknowledged for the support to The Norwegian Center for Transmission Electron Microscopy [197405], and for support through projects “MoZEES” (257653) and “SUPROX” (280868).”

References

[1] J. Kašpar, P. Fornasiero, M. Graziani, Use of ceo2-based oxides in the three-way catalysis, Catal. Today 50 (2) (1999) 285–298, https://doi.org/10.1016/S0920-5861(98)00510-0. URL, http://www.sciencedirect.com/science/article/pii/S0920586198005100.

[2] A. Alinezhadchamazketi, A.A. Khodadadi, Y. Mortazavi, A. Nemati, Catalytic evaluation of promoted ceo2-zro2 by transition, alkali, and alkaline-earth metal oxides for diesel soot oxidation, J. Environ. Sci. 25 (12) (2013) 2498–2506, https://doi.org/10.1016/S1001-0742(12)60334-9. URL, http://www.sciencedirect.com/science/article/pii/S1001074212603349.

[3] A. Trovarelli, C. de Leitenburg, M. Boaro, G. Dolcetti, The utilization of ceria in industrial catalysis, Catal. Today 50 (2) (1999) 353–367, https://doi.org/10.1016/S0920-5861(98)00515-X. URL, http://www.sciencedirect.com/science/article/pii/S092058619800515X.

[4] P.A. Crozier, R. Wang, R. Sharma, In situ environmental tem studies of dynamic changes in cerium-based oxides nanoparticles during redox processes, Ultramicroscopy 108 (11) (2008) 1432–1440, https://doi.org/10.1016/j.ultramic.2008.05.015. URL, http://www.sciencedirect.com/science/article/pii/S0304399108001782.

[5] S. Turner, S. Lazar, B. Freitag, R. Egoavil, J. Verbeeck, S. Put, Y. Strauven, G. Van Tendeloo, High resolution mapping of surface reduction in ceria nanoparticles, Nanoscale 3 (2011) 3385–3390, https://doi.org/10.1039/C1NR10510H. URL.

[6] U.M. Graham, M.T. Tseng, J.B. Jasinski, R.A. Yokel, J.M. Unrine, B.H. Davis, A. K. Dozier, S.S. Hardas, R. Sultana, E.A. Grulke, D.A. Butterfield, Invivo processing of ceria nanoparticles inside liver: impact on free-radical scavenging activity and oxidative stress, arXiv:https://chemistry-europe.onlinelibrary.wiley.com/doi/pdf/10.1002/cplu.201402080, Chem Plus Chem. 79 (8) (2014) 1083–1088, https://doi.org/10.1002/cplu.201402080. URL, https://chemistry-europe.onlinelibrary.wiley.com/doi/abs/10.1002/cplu.201402080.

[7] B. Goris, S. Turner, S. Bals, G. Van Tendeloo, Three-dimensional valency mapping in ceria nanocrystals, ACS Nano 8 (10) (2014) 10878–10884, pMID: 25286190. arXiv:10.1021/nn5047053.

[8] J.M. Perkins, S. Fearn, S.N. Cook, R. Srinivasan, C.M. Rouleau, H.M. Christen, G. D. West, R.J.H. Morris, H.L. Fraser, S.J. Skinner, J.A. Kilner, D.W. McComb, Anomalous oxidation states in multilayers for fuel cell applications, arXiv:https://onlinelibrary.wiley.com/doi/pdf/10.1002/adfm.201000279, Adv. Funct. Mater. 20 (16) (2010) 2664–2674, https://doi.org/10.1002/adfm.201000279. URL, https://onlinelibrary.wiley.com/doi/abs/10.1002/adfm.201000279.

[9] A.C. Johnston-Peck, W.-C.D. Yang, J.P. Winterstein, R. Sharma, A.A. Herzing, In situ oxidation and reduction of cerium dioxide nanoparticles studied by scanning transmission electron microscopy, Micron 115 (2018) 54–63, https://doi.org/10.1016/j.micron.2018.08.008. URL, https://www.sciencedirect.com/science/article/pii/S0968432818302361.

[10] F. Zhang, P. Wang, J. Koberstein, S. Khalid, S.-W. Chan, Cerium oxidation state in ceria nanoparticles studied with x-ray photoelectron spectroscopy and absorption near edge spectroscopy, Surf. Sci. 563 (1) (2004) 74–82, https://doi.org/10.1016/j.susc.2004.05.138. URL, https://www.sciencedirect.com/science/article/pii/S003960280400812X.

[11] J. I, J.R. L, M. Baalousha, P. Le Coustumer, Characterisation of structural and surface speciation of representative commercially available cerium oxide nanoparticles, Environ. Chem. 7 (2010) 377–385.

[12] S. Raz, K. Sasaki, J. Maier, I. Riess, Characterization of adsorbed water layers on y2o3-doped zro2, Solid State Ionics 143 (2) (2001) 181–204, https://doi.org/10.1016/S0167-2738(01)00826-8. URL, https://www.sciencedirect.com/science/article/pii/S0167273801008268.

[13] E. Mamontov, Observation of fragile-to-strong liquid transition in surface water in ceo2, J. Chem. Phys. 123 (17) (2005), 171101 arXiv:10.1063/1.2125729.

[14] A.C. Johnston-Peck, J.S. DuChene, A.D. Roberts, W.D. Wei, A.A. Herzing, Dose-rate-dependent damage of cerium dioxide in the scanning transmission electron microscope, Ultramicroscopy 170 (2016) 1–9, https://doi.org/10.1016/j.ultramic.2016.07.002. URL, https://www.sciencedirect.com/science/article/pii/S0304399116300936.

[15] Y. Wang, Q. Zhou, L. Kang, L. Yang, H. Wu, Z. Zhou, C. Xiao, J. Guo, F. Yang, S. Zhang, G. Li, Y. Jin, Oxide-water interaction and wetting property of ceria surfaces tuned by high-temperature thermal aging, Appl. Surf. Sci. 554 (2021), 149658, https://doi.org/10.1016/j.apsusc.2021.149658. URL, https://www.sciencedirect.com/science/article/pii/S0169433221007340.

[16] R. Wang, P.A. Crozier, R. Sharma, J.B. Adams, Measuring the redox activity of individual catalytic nanoparticles in cerium-based oxides, Nano Lett. 8 (3) (2008) 962–967, pMID: 18251517. arXiv:10.1021/nl073135c.